



Cite this: *Analyst*, 2015, **140**, 7997

## Efficient detection of *Escherichia coli* O157:H7 using a reusable microfluidic chip embedded with antimicrobial peptide-labeled beads

Mi-Sook Chang,<sup>†a</sup> Jeong Ha Yoo,<sup>†a,b</sup> Deok Ha Woo<sup>b</sup> and Myung-Suk Chun<sup>\*b,c</sup>

The ability of antimicrobial peptides (AMPs) for effective binding to multiple target microbes has drawn lots of attention as an alternative to antibodies for detecting whole bacteria. We investigated pathogenic *Escherichia coli* (*E. coli*) detection by applying a microfluidic based biosensing device embedded with AMP-labeled beads. According to a new channel design, our device is reusable by the repeated operation of detection and regeneration modes, and the binding rate is more enhanced due to even distribution of the bacterial suspension inside the chamber by implementing influx side channels. We observed higher binding affinity of pathogenic *E. coli* O157:H7 for AMP-labeled beads than nonpathogenic *E. coli* DH5 $\alpha$ , and the fluorescence intensity of pathogenic *E. coli* was about 3.4 times higher than the nonpathogenic one. The flow rate of bacterial suspension should be applied above a certain level for stronger binding and rapid detection by attaining a saturation level of detection within a short time of less than 20 min. A possible improvement in the limit of detection in the level of 10 cells per mL for *E. coli* O157:H7 implies that the AMP-labeled beads have high potential for the sensitive detection of pathogenic *E. coli* at an appropriate flow rate.

Received 30th June 2015,  
Accepted 19th October 2015

DOI: 10.1039/c5an01307k

www.rsc.org/analyst

### Introduction

Pathogenic bacteria detection serves as an important tool in the field of public health, including clinical diagnostics, pathology, drug discovery, disease outbreaks, food safety, and water monitoring. Although antibodies are widely utilized for the detection and quantification of pathogens,<sup>1–3</sup> it is often necessary to sacrifice a lot of animals for their production, and these antibodies have several limitations in their stability, quality-assured preparations, and cost effectiveness. The emerging alternatives to antibodies include antimicrobial peptides (AMPs),<sup>4–10</sup> real-time quantitative polymerase chain reaction (PCR),<sup>11,12</sup> primers with micro-PCR chips,<sup>13,14</sup> peptide nucleic acid (PNA) probes,<sup>15</sup> and so on.

The natural AMPs have several attractive advantages such as a broad spectrum of antimicrobial activity, increased bacterial

resistance, and reaction with a very low concentration, where their binding activity is due to their cationic and amphiphilic nature. A total positive charge accumulates at polyanionic bacterial cell surfaces that contain acidic lipopolysaccharide (LPS) and wall-connected teichoic acids in Gram-negative and Gram-positive bacteria, respectively. Subsequently, the AMPs binding to the anionic surface of the cytoplasmic membrane are inserted in a way of getting on the interface of the hydrophilic head groups and the acyl chains of membrane phospholipids.<sup>16,17</sup> Given the above advantages, AMPs have been used as a good biosensing tool to detect a variety of pathogenic agents, including bacteria, toxins, and viruses with a lipoprotein envelope. Most studies of AMPs have been conducted on magainin II until the AMP magainin I was applied as a recognition element for bacteria. Kulagina *et al.*<sup>4</sup> reported that an array with multiple AMPs could more effectively detect the target analytes of Gram-negative *E. coli* O157:H7 and *Salmonella typhimurium* than an array with antibodies. They also demonstrated stronger antimicrobial activity of magainin I than the other AMPs through the disruption of microbes' membranes.<sup>5</sup> The first effort was made by Mannoor *et al.*<sup>7</sup> to apply AMP magainin I immobilized on arrays of gold electrodes for the detection of *E. coli*, *S. typhimurium*, and Gram-positive *Listeria monocytogenes* in microfluidic flow, using impedance measurements as a label-free and portable biosensor. Moreover, the

<sup>a</sup>Laboratory of Cellular Neurobiology, Dept of Oral Anatomy, School of Dentistry & Dental Research Institute, Seoul National University, Jongno-gu, Seoul 110-749, Republic of Korea

<sup>b</sup>Sensor System Research Center, National Agenda Research Division, Korea Institute of Science and Technology (KIST), Seongbuk-gu, Seoul 136-791, Republic of Korea. E-mail: mschun@kist.re.kr; Tel: +82-2-958-5363

<sup>c</sup>Biomedical Engineering Program, Korea University of Science and Technology, Daejeon 305-350, Republic of Korea

<sup>†</sup>Authors contributed equally.

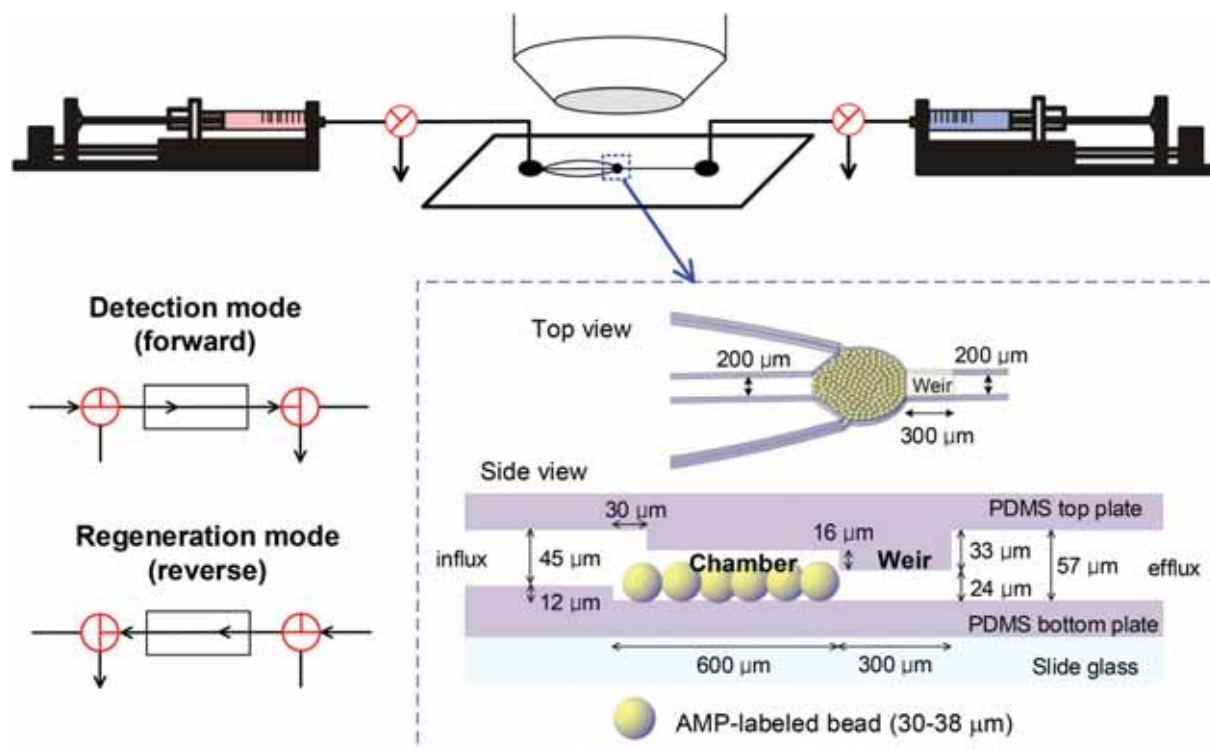


Fig. 1 Illustration of the microfluidic based biosensor for *E. coli* detection utilized in the present study. The scale does not represent the actual size.

stronger antimicrobial activity permits magainin I to be used as an AMP-coated polymer brush<sup>18</sup> and an anti-biofilm,<sup>19</sup> by testing against Gram-positive pathogens.

Microfluidic based pathogen detection offers an efficient platform in view of its miniaturization, small sample volume, portability, rapidity, and point-of-care diagnosis.<sup>20,21</sup> Microbead-based microfluidic devices have been widely used in the field of bioassay, because of their advantages in disposability, specificity, and rapid detection. Microbeads of agarose,<sup>22,23</sup> glass,<sup>2</sup> magnetic materials,<sup>3,24,25</sup> silica,<sup>26</sup> and polystyrene<sup>27</sup> were used as the support, and a pillar or a weir structure was applied inside the microchannel for effective packing of microbeads.<sup>28,29</sup> The microbeads with AMP-binding activity have the potential to become a sensitive method for bacteria detection, due to the increased surface area for binding to microorganisms compared to the geometry of flat plates. In our recent study,<sup>8</sup> a new method to detect nonpathogenic *E. coli* DH5 $\alpha$  was developed by implementing the microfluidic chip designed with a weir inside the channel, where AMP-labeled microbeads were embedded. From the analysis of detection rate and the estimation of detection efficiency, we found that our device can rapidly detect *E. coli* concentrations of  $10^3$  cells per mL (*i.e.*, 1 bacterium per  $\mu\text{L}$ ) within 30 min.

In this study, pathogenic *E. coli* O157:H7 has been detected by utilizing our microfluidic chip precisely fabricated with multiple mold layers by complex procedures. As shown in Fig. 1, it is designed with a chamber and a weir to embed AMP-labeled beads and operated periodically for detection and

regeneration. Bacterial suspension can be distributed evenly inside the chamber by the influx channel consisting of a main and two side channels. We compared the binding affinity between *E. coli* DH5 $\alpha$  and O157:H7 and characterized the detection rate with various flow rates and bacteria concentrations to examine the detection performance of our device. It presents an improvement in the limit of detection (LOD) for *E. coli* O157:H7 compared to the previous reports, implying that the AMP-labeled beads are more effective for the rapid and sensitive detection of pathogenic *E. coli* than the non-pathogenic one.

## Experimental

### Reusable microfluidic chip fabrication

Our improved microfluidic chip enables embedded AMP-labeled beads for reuse. Its channel designed by a computer-aided design program (AutoCAD-2013) was fabricated with polydimethylsiloxane (PDMS) by applying soft lithography and followed by bonding. As shown in Fig. 2, two photomasks for chamber and weir layers and another two photomasks for influx channel and efflux channel layers were prepared for the fabrications of master molds of top and bottom plates, respectively. Two influx side channels positioned at both sides of a round chamber with an angle of 75 degrees to an influx main channel so that bacterial suspension can be evenly distributed inside the whole region of the chamber. The depth of the weir

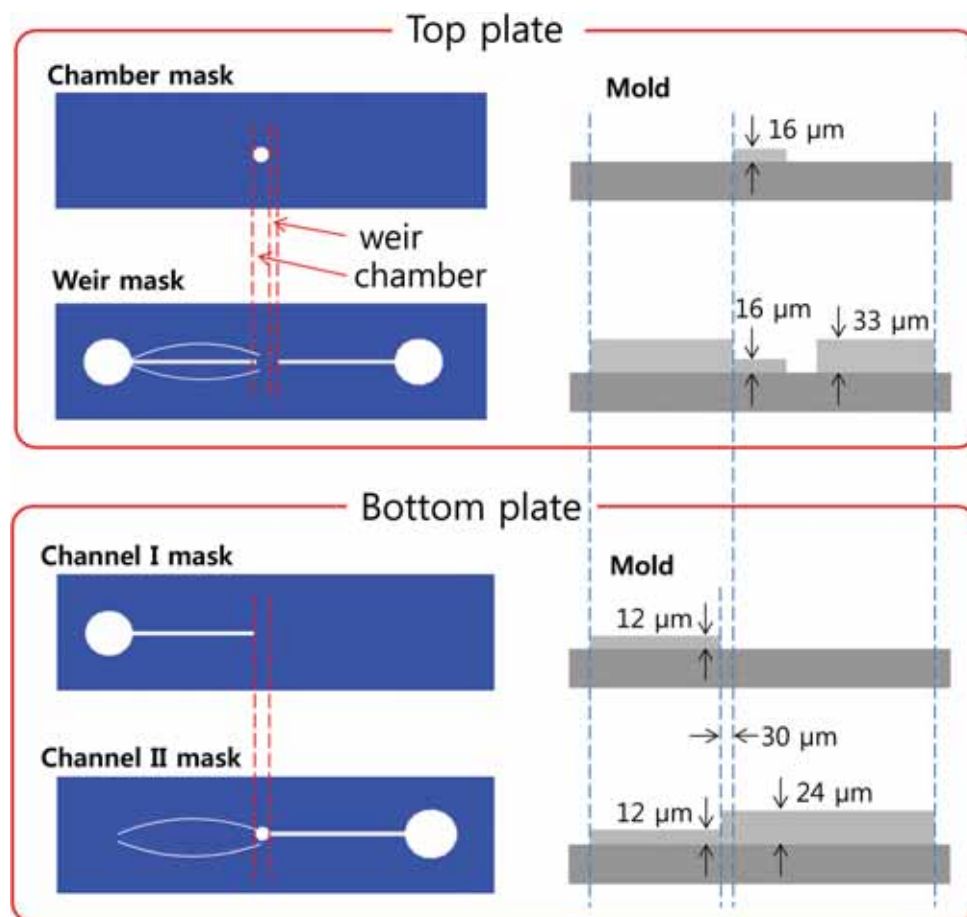


Fig. 2 CAD design of four masks for master molds of top and bottom plates and the corresponding cross-sectional side views along the centerline of molds, where each mold consists of two-layered photoresist structures on a silicon wafer. The scale does not represent the actual size.

is critical for retaining the microbeads in the chamber, and the depth of the chamber should be slightly higher than the diameter of the microbeads for packing as a monolayer. Our chip is designed to have the bottom of the influx main channel located at the front of the chamber  $12\ \mu\text{m}$  high and the width of two influx side channels narrower ( $25\ \mu\text{m}$ ) than the diameter of the beads. This design provides preventing the leakage of embedded beads during the regeneration mode by reverse flow. Here, the function of influx and efflux channels is switching in regeneration mode.

In order to create two master molds of the top and bottom plates, we applied photolithography twice with the same negative photoresists (PRs) SU-8 2015 (MicroChem, Newton, MA) and aligned the two layered sets during each corresponding process. The fabrication process is shown in Fig. 3. The photolithography consists of the 1st mold layer (top plate:  $16\ \mu\text{m}$  height, bottom plate:  $12\ \mu\text{m}$  height) patterning by chamber and channel I masks and the 2nd mold layer (top plate:  $33\ \mu\text{m}$  height, bottom plate:  $24\ \mu\text{m}$  height) patterning by weir and channel II masks. The post exposure bake was followed by the removal of unexposed PR by dissolving with the SU-8 developer and a master mold containing the negatively patterned PR

remained. The unexposed area in the weir mask for the top plate becomes the chamber and weir, and the difference in the PR heights will be translated into the different depths between the weir and chamber as well as the chamber and influx main channel.

Next, PDMS (Sylgard 184, Dow Corning, MI) mixed with the curing agent in a volume ratio of 10 : 1 was poured into each master mold, and then was cured against the master at  $80\ ^\circ\text{C}$  for at least 1 h. The peeled PDMS replica of the top plate was punched to generate holes for the inlet and outlet reservoirs, and bonded to that of the bottom plate. Subsequently, it was bonded to slide glass using an oxygen plasma generator (CUTE-1MP, FemtoScience, Korea), which was baked at  $80\ ^\circ\text{C}$  for at least 60 min and stored at room temperature (RT). Finally, Teflon tubing (ID: 0.8 mm, OD: 1.5 mm) was adhered to each reservoir.

#### Preparation of AMP-labeled beads and *E. coli* staining

We purchased the AMP magainin I (GIGKFLHSAGKFGKAFV-GEIMKS) (AnyGen, Gwangju, Korea) synthesized to contain a cysteine residue at the C-terminus with a purity >95%. The binding affinity between magainin I and *E. coli* is much lower

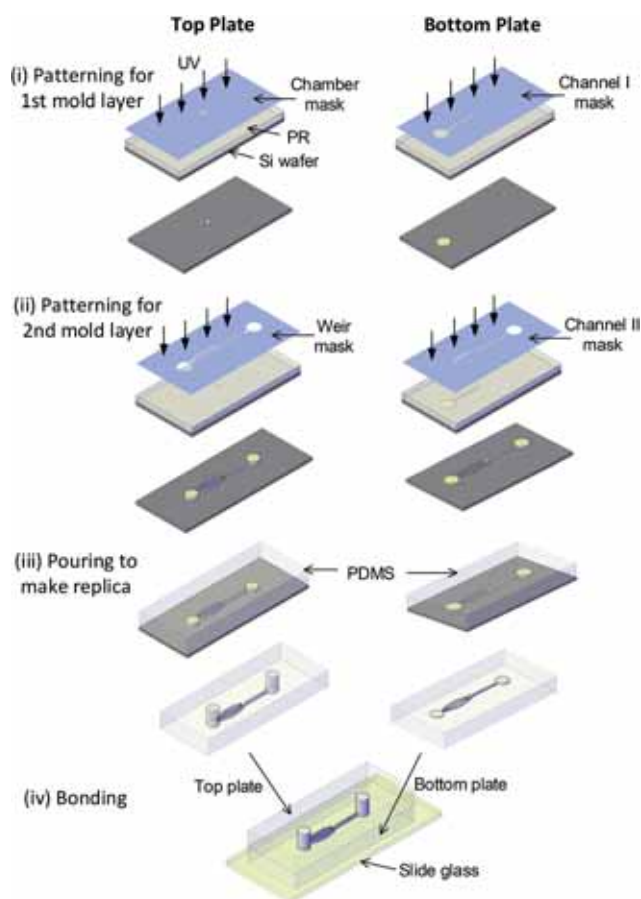


Fig. 3 Schematic of fabrication procedures of a microfluidic chip consisting of PDMS top and bottom plates and slide glass.

in N-terminal immobilization than that of the C-terminus.<sup>7</sup> Fig. 4 shows the preparation of AMP-labeled beads and the binding of *E. coli*, and details were described in our previous paper.<sup>8</sup> The primary amine-functionalized glass beads (30–38  $\mu\text{m}$  in diameter, Polysciences, PA) were incubated with 1.0 mM *N*-[ $\gamma$ -maleimidobutyryloxy] succinimide ester (GMBS; Fluka, Switzerland) in absolute ethanol for 30 min at RT, followed by rinsing and drying several times. The maleimide-activated beads were incubated overnight with 43  $\mu\text{M}$  AMP magainin I in phosphate-buffered saline (PBS, pH 7.4), cross-linking with a sulfhydryl group of a cysteine residue at the C-terminus to produce direct covalent bonding.<sup>4,5,7,19</sup> The prepared AMP-labeled beads were stored at 4  $^{\circ}\text{C}$  and used within three weeks.

Nonpathogenic *E. coli* DH5 $\alpha$  (ATCC 35218) and pathogenic *E. coli* O157:H7 (ATCC 43894) were obtained from the American Type Culture Collection (ATCC). They were grown for 16 h at 37  $^{\circ}\text{C}$  in Luria–Bertani (LB; Difco Laboratories, Spark, MD) broth, and diluted to the prescribed concentration. To compare their binding affinity for AMP, we stained *E. coli* DH5 $\alpha$  and *E. coli* O157:H7 with 3  $\mu\text{M}$  propidium iodide (PI;  $\text{C}_{27}\text{H}_{34}\text{I}_2\text{N}_4$ , Invitrogen, CA) and 0.1  $\mu\text{g ml}^{-1}$  4',6-diamidino-2-phenylindole (DAPI;  $\text{C}_{16}\text{H}_{15}\text{N}_5\cdot 2\text{HCl}$ , Santa Cruz Biotechnol-

ogy, TX), respectively, in PBS for 1 h. The AMP-labeled beads were bound to both *E. coli* through the interaction between the AMP and the bacterial surface, as shown in Fig. 4. According to a previous report,<sup>30</sup> the negatively charged LPS in the outer layer of Gram-negative bacteria (such as *E. coli*) can readily bind to the AMP, whereas Gram-positive bacteria do not readily bind to the AMP due to the absence of LPS.

The number of *E. coli* was quantified by measuring the optical density of *E. coli* culture at 600 nm ( $\text{OD}_{600}$ ) using a UV-Vis spectrophotometer (ND-2000, Thermo Scientific, DE), where  $\text{OD}_{600}$  reading of 1.0 corresponds to approximately  $8 \times 10^8$  cells per mL. For biosafety considerations, the bacteria were heated in a 100  $^{\circ}\text{C}$  heating block for 20 min before applications. Stained *E. coli* cells were observed by using a confocal microscope (FV-300, Olympus, Japan) to confirm the morphology, the cell sizes are typically several micrometers with a diameter of ca. 1  $\mu\text{m}$  and some bacteria have long tails, as found previously.

### Fluidic operation and *E. coli* binding

To embed the AMP-labeled beads, their suspension in PBS with 0.05% Triton X-100 was carefully injected into the chamber through the influx main channel using a syringe pump (Pump 11 Elite-Nanomite, Harvard Apparatus, MA). The packed beads were washed for 20 min with PBS at 5  $\mu\text{L min}^{-1}$  before the first injection of *E. coli* suspension. As shown in Fig. 1, the fluidics setup consisted of a detection mode by forward flowing of bacterial suspension and a regeneration mode by reverse flowing of a PBS solution. Each mode was properly operated by two syringe pumps and two 3-way switching valves (V101T, Upchurch, Oak Harbor, WA) were positioned upstream and downstream. The microfluidic chip was positioned on a fluorescence microscope (Eclipse Ni-U, Nikon, Japan) for monitoring and image data acquisition during operations. Images were taken by using a digital 3  $\times$  14 bit color charge-coupled device (CCD) camera (AxioCam HRC, Carl Zeiss, Germany).

Both the AMP-labeled bead and its binding with *E. coli* were observed by field emission scanning electron microscopy (FE-SEM, Hitachi, S-4700). To do this, each sample was fixed with 2% paraformaldehyde and 2.5% glutaraldehyde in PBS for 3–4 h at RT and dried in a fume hood. Then, the morphology of the binding *E. coli* on the surface of the AMP-labeled bead was observed by using a laser-scanning confocal microscope with metric image analysis, where the Z-stack images were captured at 1  $\mu\text{m}$  intervals until 14  $\mu\text{m}$  upwardness. The detected *E. coli* stained with each dye can be visualized under a fluorescence microscope.

## Results and discussion

### Binding affinity of AMP-labeled beads to *E. coli*

We first examined the binding between AMP-labeled beads and *E. coli* using SEM, as shown in Fig. 5. The magnified image of the immobilized AMP on the surface of a glass bead

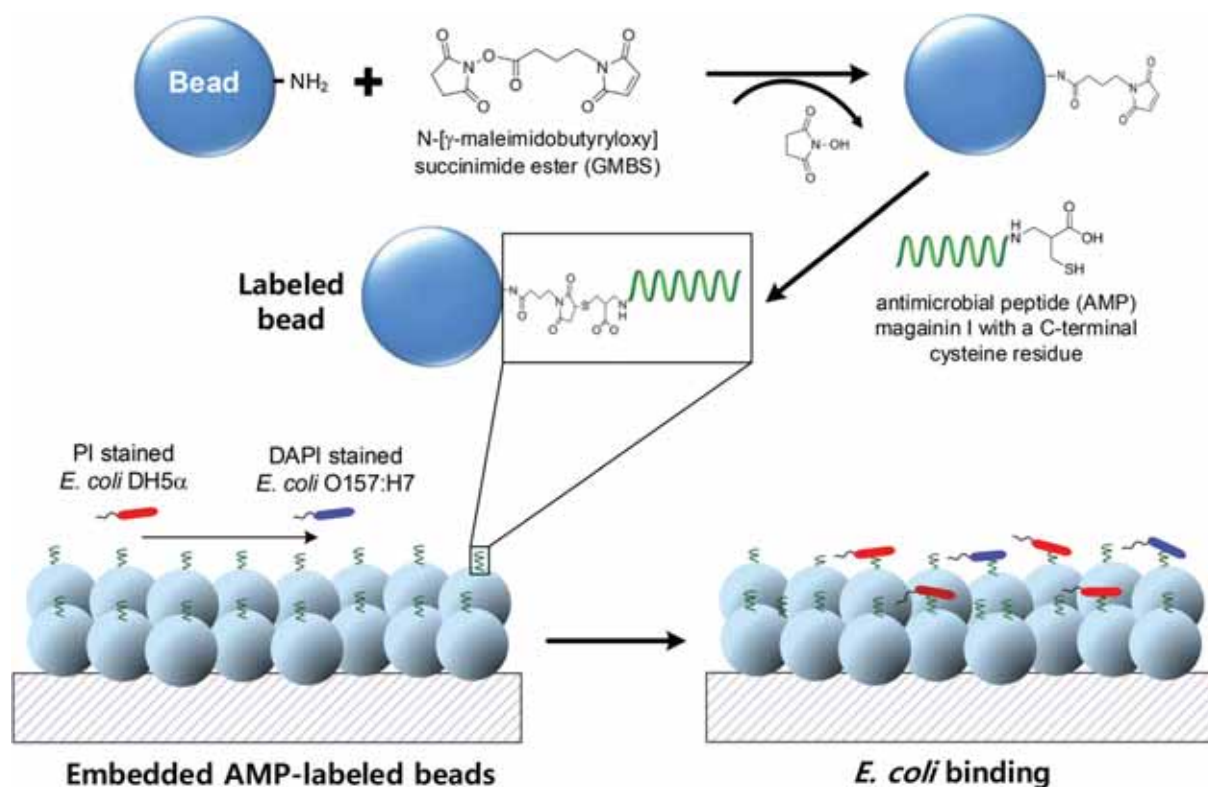


Fig. 4 Schematic representation of the immobilization of AMPs on a bead and the binding of *E. coli* to the AMP-labeled bead.

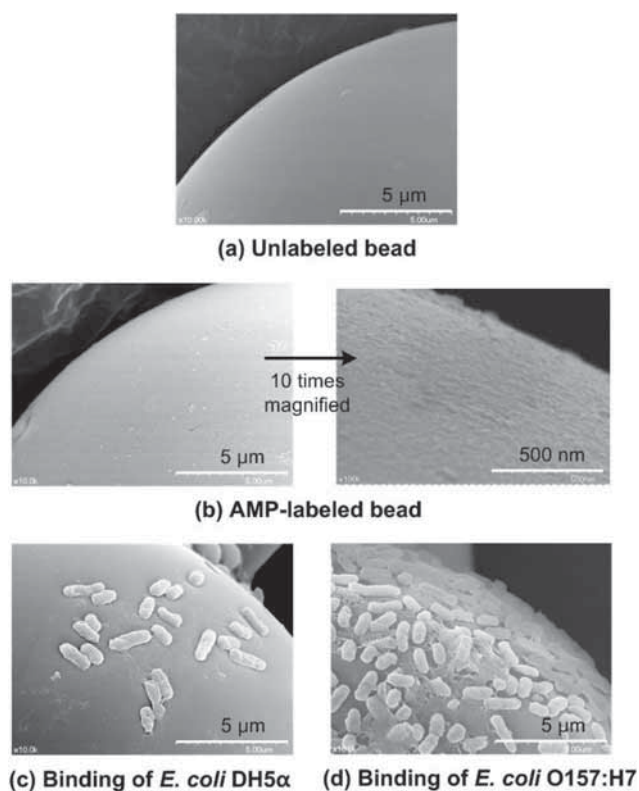


Fig. 5 SEM images of (a) unlabeled bead, (b) AMP-labeled bead, and its capturing with (c) *E. coli* DH5α cells and (d) *E. coli* O157:H7 cells.

can be seen in Fig. 5b, and the images shown in Fig. 5c and d were obtained by incubating a heat-killed *E. coli* sample ( $10^8$  cells per mL) with AMP-labeled beads for 10 min. It is evident that pathogenic *E. coli* O157:H7 binds to the surface of the AMP-labeled bead much more than nonpathogenic *E. coli* DH5α.

In Fig. 6a, compared to PI-stained *E. coli* DH5α (red color), DAPI-stained *E. coli* O157:H7 (blue color) presents stronger fluorescence intensity and larger number of stained cells bound to the surface of the AMP-labeled bead. Both results of SEM and confocal microscopy images are consistent, identifying that the binding affinity of the AMP-labeled bead is much higher for pathogenic *E. coli*. According to the selectivity and interbacterial strain differentiation reported in the literature,<sup>7</sup> magainin I exhibits preferential binding toward the pathogenic *E. coli* relative to the nonpathogenic one, with 1.5–2 orders of magnitude difference in impedance.

Fig. 6b shows the changes in fluorescence images at the initial stage of 1 min and almost saturated stage of 10 min, where each bacteria concentration is  $5 \times 10^3$  cells per mL. The dye-stained *E. coli* was detected by adopting 522–560 nm excitation and 575–665 nm emission filters for PI ( $\lambda_{\text{ex}} = 535$  nm,  $\lambda_{\text{em}} = 617$  nm) and 350–400 nm excitation and 390–500 nm emission filters for DAPI ( $\lambda_{\text{ex}} = 358$  nm,  $\lambda_{\text{em}} = 461$  nm). As described in our previous study,<sup>8</sup> during the progress of the bacteria detection, there exists nonspecific binding caused by interspaces between the beads as well as between the beads

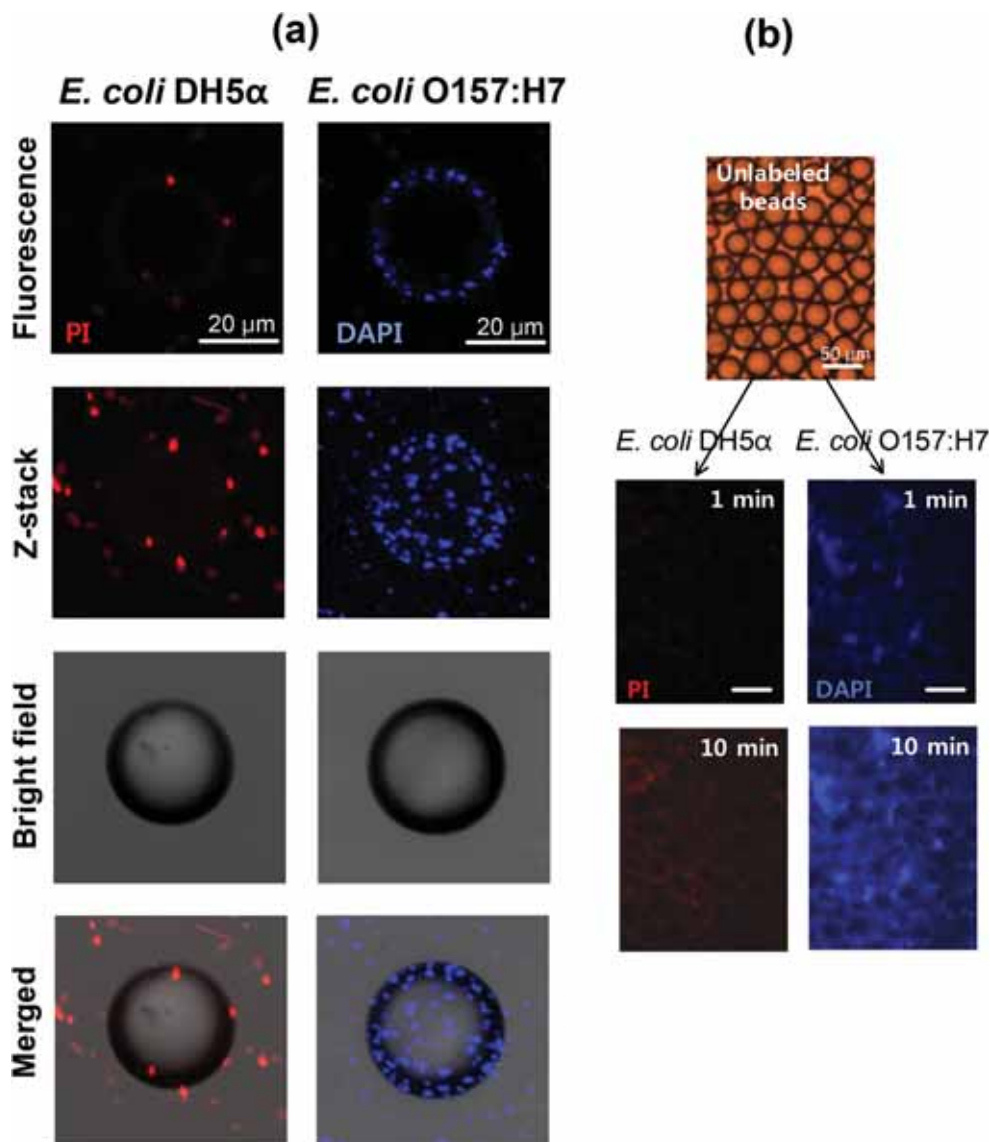


Fig. 6 (a) Confocal microscopy images of PI- and DAPI-stained *E. coli* bound to AMP-labeled beads, (b) changes in fluorescence images by detecting *E. coli* DH5 $\alpha$  and *E. coli* O157:H7 ( $5 \times 10^3$  cells per mL) at times of 1 and 10 min for  $2 \mu\text{L min}^{-1}$ .

and the microchannel wall, in addition to the specific binding between the surface of *E. coli* and the AMP-labeled beads. Non-specific binding can be observed in the fluorescence images of the channel embedded with unlabeled beads (data not shown here). In this study, we present the total binding caused by both nonspecific and specific binding. The colored image represents the detected *E. coli* on the surface of the beads, in which detecting *E. coli* O157:H7 by binding strongly develops as time progresses.

#### Detection and regeneration of AMP-labeled beads

The electrostatic interaction is involved in binding affinity between *E. coli* and AMP magainin I. This indicates the possibility of detaching *E. coli* bound to AMP magainin I by washing with PBS solution at high flow rates in the regener-

ation mode (*cf.* Fig. 1), which allows the microfluidic chip to be reused. From the preliminary tests with our chip, we found that the washing flow rate of less than  $15 \mu\text{L min}^{-1}$  took more than 1 h to completely detach the *E. coli*, whereas the washing flow rate more than  $24 \mu\text{L min}^{-1}$  resulted in a disordered monolayer due to displacements of beads. Thus, the washing flow rate was suitably determined as  $20 \mu\text{L min}^{-1}$ .

Fig. 7a shows real-time monitoring of the fluorescence intensity ( $I$ ) of *E. coli* DH5 $\alpha$  and O157:H7 according to total detection as the time proceeds with repeated operation of detection mode ( $2 \mu\text{L min}^{-1}$ ) for 30 min followed by regeneration mode ( $20 \mu\text{L min}^{-1}$ ) for 40 min. An *E. coli* concentration of  $5 \times 10^3$  cells per mL in feed suspension was applied by considering our previous results of detection efficiency. All data are averages from three replicate experiments, and error bars

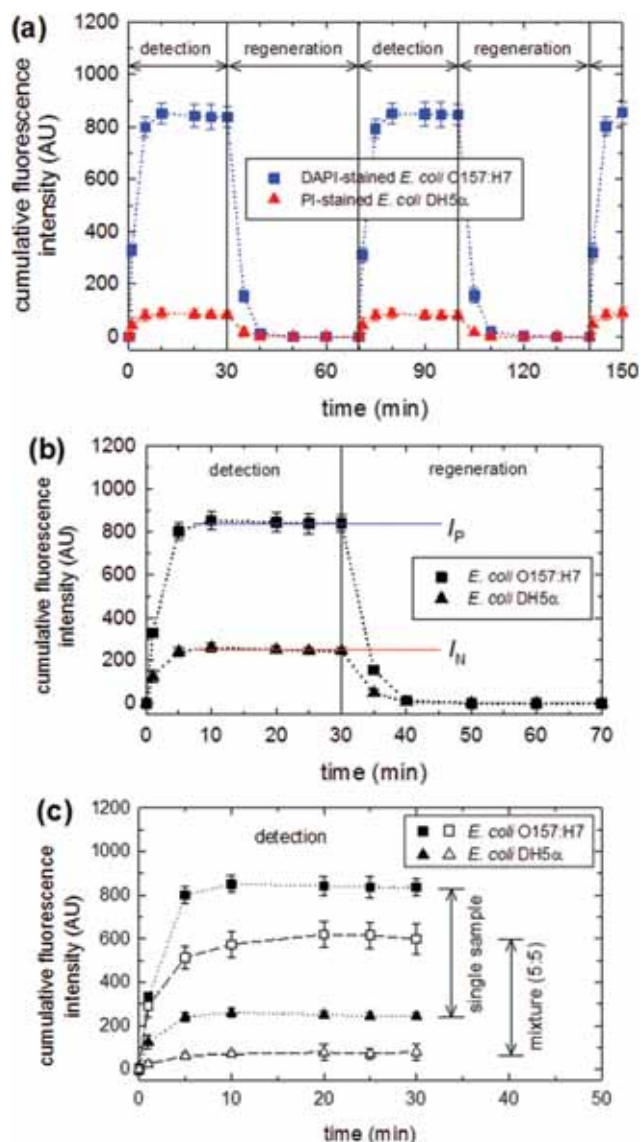


**Fig. 7** Real-time monitoring of total detection for different fluorescence intensities (a) between PI- and DAPI-stained *E. coli* and (b) between these *E. coli* correct to DAPI staining, as the time proceeds. (c) Shows comparisons between single samples and their mixture of equal concentration. Each bacteria concentration was  $5 \times 10^3$  cells per mL and flow rates for detection and regeneration modes were set as 2 and  $20 \mu\text{L min}^{-1}$ , respectively. Error bars indicate standard deviations for three replicate experiments.

indicate their standard deviations. The cumulative fluorescence intensity was obtained using the ImageJ (National Institute of Health, MD) program for inverted images without the background, and an intensity threshold was applied to estimate the fluorescent area. We point out that saturation of each fluorescence within 10 min and complete washing by regeneration for 40 min provide the validity of our reusable microfluidic chip.

Fluorescence intensities of both PI- and DAPI-stained *E. coli* DH5 $\alpha$  were estimated by obtaining these fluorescence images

under the same conditions, and found out that  $I_{\text{DAPI}}/I_{\text{PI}} = 2.92$ . Accordingly, we corrected the cumulative fluorescence intensity of PI-stained DH5 $\alpha$  to that of DAPI-stained one so as to exclude the variation of  $I$  depending on the staining dye, as shown in Fig. 7b. The fluorescence intensity based on DAPI can be obtained by averaging each intensity during steady state detection for 10–30 min. As a result, we found that the fluorescence intensity of pathogenic *E. coli* O157:H7 (*cf.*  $I_{\text{P}} = 842$ ) is 3.4 times higher than that of nonpathogenic *E. coli* DH5 $\alpha$  (*cf.*  $I_{\text{N}} = 249$ ). This result corresponds to the images of SEM and confocal microscopy. Fig. 7b is useful in estimating the unknown concentrations of nonpathogenic and pathogenic *E. coli* (*i.e.*, volume fraction  $X_{\text{N}}$  and  $X_{\text{P}}$ , respectively) in a test sample with the fluorescence intensity  $I_{\text{sample}}$  ( $I_{\text{N}} \times X_{\text{N}} + X_{\text{P}} \times I_{\text{P}}$ ) for volume  $V_{\text{sample}}$ . Since  $X_{\text{N}} + X_{\text{P}} = 1$  and  $I_{\text{sample}} = X_{\text{N}}I_{\text{N}} + X_{\text{P}}I_{\text{P}}$  by the assumption of the linear relationship between the bacterial concentration and the fluorescence intensity, it is possible to finally obtain each concentration of *E. coli*.

Fig. 7c shows the fluorescence intensities for a mixture of *E. coli* O157:H7 and DH5 $\alpha$  in equal concentrations of  $5 \times 10^3$  cells per mL each, which decreased compared to the corresponding fluorescence intensities for the single sample. Here,  $|I_{\text{P}} - I_{\text{N}}|$  can represent the specificity between *E. coli* O157:H7 and DH5 $\alpha$ .  $|I_{\text{P}} - I_{\text{N}}|$  for the mixture is slightly smaller than that for the single sample, meaning a little decrease in the specificity. We performed further experiments for mixtures with other concentration ratios of these bacteria (*cf.* 5 : 1, 1 : 5, and 0.5 : 5) to examine the change of specificity (not shown here). Specificity changes are complicated in the mixture depending on the concentration ratios, due to a difference in binding affinity between these *E. coli* and its interfering effect.

### Performance of pathogenic *E. coli* detection

In order to verify the performance of *E. coli* O157:H7 detection, we need to examine the effect of flow rate. Flow conditions can be quantified by considering the velocity field at the steady state laminar flow in a microchannel of rectangular cross-section with height  $H$  and width  $W$ . For the flow rate  $Q$  of Newtonian fluids with pressure difference  $\Delta P$  along the length  $L$ , its analytical solution is available as<sup>31</sup>

$$Q \equiv v_{\text{m}}(WH) = \frac{WH^3 \Delta P}{12\mu L} \left[ 1 - \frac{192 H}{\pi^5 W} \sum_{n=\text{odd}} \frac{1}{n^5} \tanh(n\pi W/2H) \right] \quad (1)$$

where  $v_{\text{m}}$  is the average velocity and  $\mu$  is the viscosity of suspension or solution. Microfluidic behavior is characterized by the Reynolds number (Re), defined as

$$\text{Re} = \frac{\rho_f D_h v_{\text{m}}}{\mu} \quad (2)$$

where  $\rho_f$  is the density of suspension or solution and the equivalent hydraulic diameter  $D_h$  of the channel is  $2WH/(W + H)$ . Table 1 summarizes the hydrodynamic conditions estimated at the influx main channel and at the weir with variations in flow rates.

Table 1 Hydrodynamic conditions applied in this study

Mode	Flow rate, $Q$ ( $\mu\text{L min}^{-1}$ )	At the influx main channel			At the weir		
		$v_m$ ( $\text{mm s}^{-1}$ )	$\Delta P/L$ (bar/mm)	Re (-)	$v_m$ ( $\text{mm s}^{-1}$ )	$\Delta P/L$ (bar/mm)	Re (-)
Detection	0.05	0.074	$5.11 \times 10^{-6}$	0.005	0.17	$3.92 \times 10^{-5}$	0.007
	0.5	0.741	$5.11 \times 10^{-5}$	0.054	1.74	$3.92 \times 10^{-4}$	0.074
	2.0	2.98	$2.06 \times 10^{-4}$	0.219	6.94	$1.57 \times 10^{-3}$	0.298
	4.0	5.97	$4.12 \times 10^{-4}$	0.438	13.9	$3.13 \times 10^{-3}$	0.595
Regeneration <sup>a</sup>	20	29.8	$2.06 \times 10^{-3}$	2.19	69.4	$1.57 \times 10^{-2}$	2.98

<sup>a</sup> Due to the reverse flow, the influx channel functions as the efflux channel.

In Fig. 8a, the range of flow rate for detection mode verifies that Re is in the typical order of the microfluidic system. The flow rate is inversely proportional to the residence time in the void space of the bead packing zone, which directly affects the binding of *E. coli* to the beads.<sup>8</sup> At a lower flow rate of  $0.05 \mu\text{L min}^{-1}$ , the cumulative fluorescence intensity of DAPI-stained *E. coli* O157:H7 varies in an unstable manner so that the detec-

tion rate becomes very slow. The relationship between the fluorescence intensity and the time progress represents an exponential rise with flow rates of above  $0.5 \mu\text{L min}^{-1}$ . An excessive flow condition of  $4 \mu\text{L min}^{-1}$  results in early detection of saturation but weakens the binding capacity due to a deficient residence time, which is not long enough for the efficient binding between *E. coli* and the beads. Applying  $2 \mu\text{L min}^{-1}$  reaches also shortly the saturation level and allows to attain rapid detection, because other microfluidic based biosensors take more than 1 h to detect the target *E. coli*.<sup>6,7,11,12</sup> Note that, compared to our previous chip with straight weir geometry, the current chip enables achieving longer retention time as well as even distribution of bacterial suspension for efficient binding by designing a round chamber with influx side channels. Moreover, it realizes the enhanced *E. coli* contact to the surface of the bead by reducing the height of the chamber to  $40 \mu\text{m}$ .

We also examined the time evolution of total detection with various concentrations of *E. coli*, as shown in Fig. 8b. Lower concentration represents the lower fluorescence intensity, and

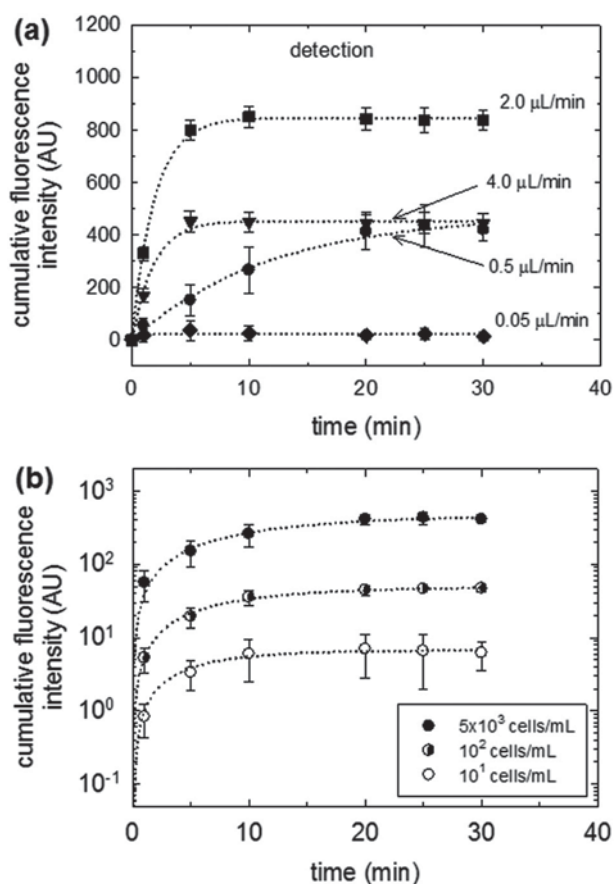


Fig. 8 Time evolution of total detection of *E. coli* O157:H7 for detection mode (a) at  $5 \times 10^3$  cells per mL with various flow rates ( $0.05$ – $4.0 \mu\text{L min}^{-1}$ ) and (b) at a flow rate of  $0.5 \mu\text{L min}^{-1}$  with various concentrations of bacteria ( $10$ – $5 \times 10^3$  cells per mL). Dotted curves are obtained by the best fits for data, and error bars not shown are smaller than the symbol size.

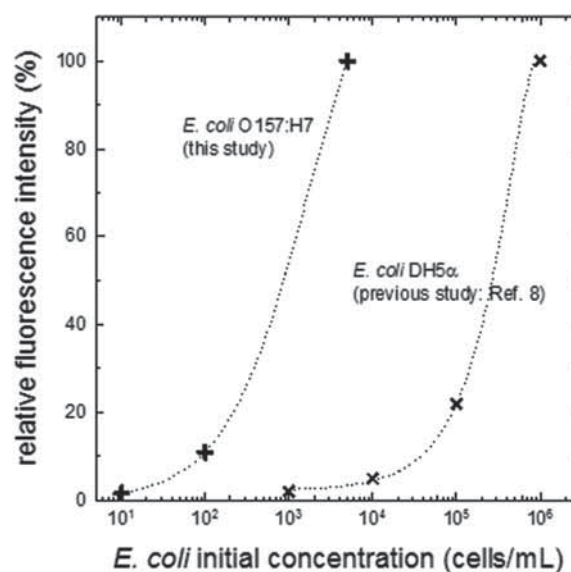


Fig. 9 The relative fluorescence intensity versus *E. coli* initial concentrations.



the fluorescence intensity is almost saturated in the range of 10 to 20 min, from which the appropriate detection time can be applied. The fluorescence intensity of concentrations less than 10 cells per mL can be predicted, if we consider the saturated fluorescence intensity for each concentration that is normalized by the saturation value for  $5 \times 10^3$  cells per mL, as shown in Fig. 9. However, a change in the relative fluorescence intensity remains quite slow for the concentrations of less than 10 cells per mL. The LOD is represented as the smallest amount of quantity of interest which produces a measurable output signal, suggesting that this level can be nearly an LOD for DAPI-stained *E. coli* O157:H7 in our chip with a newly designed channel. This level is clearly lower compared to an LOD of  $10^3$  cells per mL for PI-stained *E. coli* DH5 $\alpha$  obtained in our previous study.<sup>8</sup> We believe that our results have the potential to develop efficient biosensors, but the detection of bacteria in a real sample remains as a future study.

## Conclusions

In order to detect whole *E. coli*, we developed a reusable microfluidic chip embedded with AMP-immobilized glass microbeads on the basis of the binding activity between the beads and bacteria. Repeated operations of detection and regeneration are achieved by new channel design, and the use of microbeads enables a microfluidic device to enhance its detection efficiency by increasing the surface to volume ratio for immobilization. The SEM and confocal microscopy images show that pathogenic *E. coli* has stronger binding than nonpathogenic *E. coli*. Accordingly, the fluorescence intensity was about 3.4 times higher in pathogenic *E. coli* than the nonpathogenic one, which was observed by the total detection rate. Our data regarding the cumulative fluorescence intensity will be useful in developing a real-time and low-cost detection technique as well as estimating the unknown concentrations of nonpathogenic and pathogenic bacteria in a test sample.

The flow rate of bacterial suspension should be applied above a certain level to maintain higher binding and rapid detection by attaining a saturation level of detection in less than 20 min, but an excessive flow rate weakens the binding due to a deficient residence time. The AMP-labeled bead results in better LOD (level of 10 cells per mL) for *E. coli* O157:H7, implying that it can be applied for the rapid and sensitive detection of pathogenic *E. coli* with our device useful in dealing with bacterial cells of low concentrations close to the LOD.

## Acknowledgements

This work was supported by the Korean Health Technology R&D Project (Grant No.: A120476) from the Ministry of Health & Welfare and by the Public Welfare & Safety Research Program (2010-0020792) through the National Research Foundation (NRF) of Korea.

## References

- 1 D. A. Boehma, P. A. Gottlieb and S. Z. Hua, On-chip microfluidic biosensor for bacterial detection and identification, *Sens. Actuators, B*, 2007, **126**, 508–514.
- 2 X. Guan, H.-J. Zhang, Y.-N. Bi, L. Zhang and D.-L. Hao, Rapid detection of pathogens using antibody-coated microbeads with bioluminescence in microfluidic chips, *Biomed. Microdevices*, 2010, **12**, 683–691.
- 3 O. Laczka, J.-M. Maesa, N. Godino, J. del Campo, M. Fougthansen, J. P. Kutter, D. Snakenborg, F.-X. Muñoz-Pascual and E. Baldrich, Improved bacteria detection by coupling magneto-immunocapture and amperometry at flow-channel microband electrodes, *Biosens. Bioelectron.*, 2011, **26**, 3633–3640.
- 4 N. V. Kulagina, M. E. Lassman, F. S. Ligler and C. R. Taitt, Antimicrobial peptides for detection of bacteria in biosensor assays, *Anal. Chem.*, 2005, **77**, 6504–6508.
- 5 N. V. Kulagina, K. M. Shaffer, G. P. Anderson, F. S. Ligler and C. R. Taitt, Antimicrobial peptide-based array for *Escherichia coli* and *Salmonella* screening, *Anal. Chim. Acta*, 2006, **575**, 9–15.
- 6 S. Arcidiacono, P. Pivarnik, C. M. Mello and A. Senecal, Cy5 labeled antimicrobial peptides for enhanced detection of *Escherichia coli*, O157:H7, *Biosens. Bioelectron.*, 2008, **23**, 1721–1727.
- 7 M. S. Mannoor, S. Zhang, A. J. Link and M. C. McAlpine, Electrical detection of pathogenic bacteria via immobilized antimicrobial peptides, *Proc. Natl. Acad. Sci. U. S. A.*, 2010, **107**, 19207–19212.
- 8 J. H. Yoo, D. H. Woo, M.-S. Chang and M.-S. Chun, Microfluidic based biosensing for *Escherichia coli* detection by embedding antimicrobial peptide-labeled beads, *Sens. Actuators, B*, 2014, **191**, 211–218.
- 9 R. R. Silva, K. Y. P. S. Avelino, K. L. Ribeiro, O. L. Franco, M. D. L. Oliveira and C. A. S. Andrade, Optical and dielectric sensors based on antimicrobial peptides for microorganism diagnosis, *Front. Microbiol.*, 2014, **5**, 443.
- 10 Z.-M. Dong and G.-C. Zhao, Label-free detection of pathogenic bacteria via immobilized antimicrobial peptides, *Talanta*, 2015, **137**, 55–61.
- 11 U. Dharmasiri, M. A. Witek, A. A. Adams, J. K. Osiri, M. L. Hupert, T. S. Bianchi, D. L. Roelke and S. A. Soper, Enrichment and detection of *Escherichia coli*, O157:H7 from water samples using an antibody modified microfluidic chip, *Anal. Chem.*, 2010, **82**, 2844–2849.
- 12 K. Yamanaka, M. Saito, K. Kondoh, M. M. Hossain, R. Koketsu, T. Sasaki, N. Nagatani, K. Ikuta and E. Tamiya, Rapid detection for primary screening of influenza A virus: microfluidic RT-PCR chip and electrochemical DNA sensor, *Analyst*, 2011, **136**, 2064–2068.
- 13 C. Liu, E. Geva, M. Mauk, X. Qiu, W. R. Abrams, D. Malamud, K. Curtis, S. M. Owen and H. H. Bau, An isothermal amplification reactor with an integrated isolation membrane for point-of-care detection of infectious diseases, *Analyst*, 2011, **136**, 2069–2076.

- 14 K.-Y. Hwang, S.-Y. Jeong, Y.-R. Kim, K. Namkoong, H.-K. Lim, W.-S. Chung, J.-H. Kim and N. Huh, Rapid detection of bacterial cell from whole blood: Integration of DNA sample preparation into single micro-PCR chip, *Sens. Actuators, B*, 2011, **154**, 46–51.
- 15 B. Lam, Z. Fang, E. H. Sargent and S. O. Kelley, Polymerase chain reaction-free, sample-to-answer bacterial detection in 30 minutes with integrated cell lysis, *Anal. Chem.*, 2011, **84**, 21–25.
- 16 R. E. W. Hancock and H.-G. Sahl, Antimicrobial and host-defense peptides as new anti-infective therapeutic strategies, *Nat. Biotechnol.*, 2006, **24**, 1551–1557.
- 17 K. A. Brogden, Antimicrobial peptides: Pore formers or metabolic inhibitors in bacteria?, *Nat. Rev. Microbiol.*, 2005, **3**, 238–250.
- 18 K. Glinel, A. M. Jonas, T. Jouenne, J. Leprince, L. Galas and W. T. S. Huck, Antibacterial and antifouling polymer brushes incorporating antimicrobial peptide, *Bioconjugate Chem.*, 2009, **20**, 71–77.
- 19 V. Humblot, J.-F. Yala, P. Thebault, K. Boukerma, A. Hequet, J.-M. Berjeaud and C.-M. Pradier, The antibacterial activity of magainin I immobilized onto mixed thiols self-assembled monolayers, *Biomaterials*, 2009, **30**, 3503–3512.
- 20 A. M. Foudeh, T. F. Didar, T. Veres and M. Tabrizian, Microfluidic designs and techniques using lab-on-a-chip devices for pathogen detection for point-of-care diagnostics, *Lab Chip*, 2012, **12**, 3249–3266.
- 21 Y.-S. Lin, M.-Y. Lee, C.-H. Yang and K.-S. Huang, Biomedical devices for pathogen detection using microfluidic chips, *Curr. Proteomics*, 2014, **11**, 116–120.
- 22 Y. Yang, S.-W. Nam, N. Y. Lee, Y. S. Kim and S. Park, Superporous agarose beads as a solid support for microfluidic immunoassay, *Ultramicroscopy*, 2008, **108**, 1384–1389.
- 23 N. Buffi, D. Merulla, J. Beutier, F. Barbaud, S. Beggah, H. van Lintel, P. Renaud and J. R. van der Meer, Development of a microfluidics biosensor for agarose-bead immobilized *Escherichia coli* bioreporter cells for arsenite detection in aqueous samples, *Lab Chip*, 2011, **11**, 2369–2377.
- 24 N. Beyor, T. S. Seo, P. Liu and R. A. Mathies, Immunomagnetic bead-based cell concentration microdevice for dilute pathogen detection, *Biomed. Microdevices*, 2008, **10**, 909–917.
- 25 J. Qiu, Y. Zhou, H. Chen and J.-M. Lin, Immunomagnetic separation and rapid detection of bacteria using bioluminescence and microfluidics, *Talanta*, 2009, **79**, 787–795.
- 26 N. Bao, B. Jagadeesan, A. K. Bhunia, Y. Yao and C. Lu, Quantification of bacterial cells based on autofluorescence on a microfluidic platform, *J. Chromatogr., A*, 2008, **1181**, 153–158.
- 27 J. G. Kralj, C. Arya, A. Tona, T. P. Forbes, M. S. Munson, L. Sorbara, S. Srivastava and S. P. Forry, A simple packed bed device for antibody labelled rare cell capture from whole blood, *Lab Chip*, 2012, **12**, 4972–4975.
- 28 K. Sato, M. Tokeshi, T. Odake, H. Kimura, T. Ooi, M. Nakao and T. Kitamori, Integration of an immunosorbent assay system: analysis of secretory human immunoglobulin A on polystyrene beads in a microchip, *Anal. Chem.*, 2000, **72**, 1144–1147.
- 29 Y. Murakami, T. Endo, S. Yamamura, N. Nagatani, Y. Takamura and E. Tamiya, On-chip micro-flow polystyrene bead-based immunoassay for quantitative detection of tacrolimus (FK506), *Anal. Biochem.*, 2004, **334**, 111–116.
- 30 F. R. Rana, E. A. Macias, C. M. Sultany, M. C. Modzrakowski and J. Blazyk, Interactions between magainin 2 and *Salmonella typhimurium* outer membranes: Effect of lipopolysaccharide structure, *Biochemistry*, 1991, **30**, 5858–5866.
- 31 H. Bruus, *Theoretical Microfluidics*, Oxford University Press, New York, 2008.